Research Article

Journal of Environmental And Sciences (ISSN 2836-2551)

Synthesis and antibacterial properties of core-shell nano-ZnFe2O4@ZnS/Cu2S composites.

Xinli Zhou[a], Huihui Chen[b], Jiawei Wang[b], Miao Wu[b], Ruiling Hu[b], Junpeng Yang[b], Tinghui Qiang[a], Huan Mou[a], Xingguo Du[a], Fei Gao[a], Zhongshang Guo,[a*]

a. Department of Osteoarticular Surgery Department, Hanzhong Central Hospital, Hanzhong 723000, Shaanxi, China.
b. Shaanxi Key Laboratory of Catalysis, School of Chemical & Environment Science, Shaanxi University of Technology, Hanzhong 723000, Shaanxi, China.

***Corresponding author**

Zhongshang Guo ,
Department of Osteoarticular Surgery Department, Hanzhong Central Hospital, Hanzhong 723000, Shaanxi, China.
Email : guozhongshang001@163.com

Received Date : July 17, 2024
Accepted Date : July 18, 2024
Published Date : July 17, 2024

ABSTRACT

In recent years, the widespread use of antibiotics has led to the emergence of numerous drug-resistant bacteria, posing a severe threat to both human health and the economy. As a result, it is imperative to develop efficient antibacterial agents that do not induce drug resistance. This study employed layer-by-layer assembly technology to prepare ZnFe2O4@ZnS/Cu2S nanocomposites, which were systematically characterized using transmission electron microscopy, X-ray diffraction, X-ray photoelectron spectroscopy, energy dispersive spectroscopy, and Fourier-transform infrared spectroscopy. Gram-negative Escherichia coli (E. coli), Gram-positive Staphylococcus aureus (S. aureus) and drug-resistant Salmonella (T-Salmonella) were utilized as test bacteria to investigate the antibacterial effectiveness and mechanism of ZnFe2O4@ZnS/Cu2S. The findings demonstrated that, the MIC of the ZnFe2O4@ZnS/Cu2S against E. coli, S. aureus and T-Salmonella were 50, 60 and 80 μg/mL, respectively; At a material concentration of 200 μg/mL and a reaction time of 80 min, ZnFe2O4@ZnS/Cu2S demonstrated a bacteriostatic rate of 99.99% against the three tested bacteria. The nano-composite can disrupt cell walls and plasma membranesand effectively and resulting in bacterial rupture and demise. Furthermore, the nano-composite displayed strong biocompatibility which, together with its superior antibacterial effects, indicate significant potential for its application in medical materials and other areas of research.

Keywords: ZnFe2O4; ZIF-8; nano-composites; bacteriostatic materials; antibacterial mechanism;

1. INTRODUCTION

Bacterial infection presents a major health challenge for humans. Organic antibiotics have been crucial in curbing the spread of bacterial infections in recent decades [1]. Typically, organic bacteriostats target active enzymes, functional proteins, and organelles that are essential for bacterial transcription and translation to achieve their antibacterial effects. However, the overuse of antibiotics has led to the emergence of drug resistant in bacteria through external acquisition or their own evolution, resulting in a gradual loss of efficacy of the organic bacteriostats [2]. Hence, there is an urgent need for the development of effective antibacterial agents with low toxicity and the ability to inactivate drug-resistant bacteria as a substitute for organic antibiotics.

Copper, zinc and other inorganic metal nanoparticles have been extensively researched due to their potent and broad-spectrum antibacterial activity, as well as their low potential for drug resistance [3]. These nanoparticles interact with negative charges on bacterial cell walls and membranes and release metal ions that alter protein secondary structures and cause irreversible damage to the bacteria. Trace metal ions can diffuse into the bacterial cell and react with various cellular organelles and components, including mitochondria, nucleic acids, and plasmids, resulting in antibacterial effects [4]. Blanca and colleagues [5] investigated the antibacterial properties of ZnFe2O4 and showed that when dispersed in agar plates at a concentration of 27 mg/mL, it inhibited the growth of Staphyllococcus epidermidis by 100% and Pseudomonas aeruginosa by 67%. Chaliha evaluated the antimicrobial properties of different variants of Cu:ZnS nanosystems in disc diffusion assay against Gram-positive and Gram-negative bacteria. The results showed that the synthesised Cu:ZnS variants possessed good antibacterial activity[6] Moreover, the antibacterial activity was found to

increase with higher levels of Zn2+. Compared to several other nanomaterials, ZnFe2O4 nanoparticles have demonstrated notable contributions to biomedical applications, thanks to their remarkable biocompatibility [7]. But the antibacterial activity of nano-ZnFe2O4 alone is limited. Researchers, including Awais [8] discovered that the addition of Cu particles to ZnO NP resulted in exceptional antibacterial activity against both E. coli and S. aureus. This effect was mainly due to the combination of Cu and Zn ions. Therefore, the antibacterial properties of ZnFe2O4 nanoparticles can be enhanced by compounding Cu-based antibacterial agents.

The organic antibacterial agent ZIF-8 is a prototypic representative of zeolite-imidazolium framework (ZIFs) metal-organic frameworks (MOFs), and its exceptional performance can be applied by using it as a coating on the carrier surface [9]. The zinc (Zn2+) ion at the coordination center of the skeleton has powerful antibacterial activity while also serving as the source of copper for the generation of composite materials. The present study describes the development of a novel nano-composite bacteriostatic agent consisting of ZnFe2O4@ZnS/Cu2S. The copper source was incorporated through in-situ self-assembly of ZIF-8 on the surface of the structure, followed by calcination at 200°C. The Gram-negative bacterium E. coli, Gram-positive bacterium S. aureus and drug-resistant bacterium Salmonella T-Salmonella were utilized as test bacteria. The study investigated the synergistic antibacterial efficacy and the potential antibacterial mechanism of the nanocomposites using Bordeaux solution and zineb as controls.

2. EXPERIMENTAL MATERIALS AND METHODS

2.1. Materials

Ferric chloride hexahydrate (FeCl3•6H2O) was obtained from Tianjin Damao Chemical Reagent Factory Co., Ltd. (China). Zinc chloride and ethylene glycol, anhydrous ethanol, sodium citrate and anhydrous sodium acetate were purchased from Tianjin Tianli Chemical Reagent Co., Ltd. (China). The chemical reagent, polyvinylpyrrolidone (PVP), was provided by Tianjin Obokai Chemical Co. Limitless Chemicals, Inc. (China) together with 2-methyl-imidazole, sodium disulfide nonahydrate (Na2S•9H2O), zinc nitrate hexahydrate (Zn(NO)3•6H2O), copper nitrate trihydrate (Cu(NO3)2•3H2O), methanol, anhydrous ethanol, Zineb, Bordeaux liquid, pancreatic peptone, agar and yeast soaking powder (Shanghai Zhanyun Chemical Co., Inc.). The products were tested on E. coli (BNC-C133264), S. aureus (BNCC186335) and T-Salmonella (CCTCCB 20082358) (Shaanxi Edible Fungi Research Institute).

2.2. Material Preparation

2.2.1. Preparation of ZnFe2O4

Sixty milliliters of FeCl3•6H2O (0.12 mol/L) were dissolved in 60 mL of ethylene glycol and ultrasonicated uniformly, after which 60 mL of ZnCl2 (0.06 mol/L) was added and ultrasonicated for 30 min, after which 0.6 g sodium citrate and 3.6 g anhydrous sodium acetate were added into the reaction system and ultrasonicated for 2 h. The solution was then transferred to a reaction vessel at 200°C for 10 h, after which the precipitate containing the product was magnetically separated and washed three times with distilled water and once with anhydrous ethanol and finally dried and set aside.

2.2.2. Preparation of ZnFe2O4@ZIF-8 (ZZ)

Six hundred milligrams of ZnFe2O4 were accurately weighed out, dissolved in 150 mL of methanol, and ultrasonicated to ensure uniform mixing. PVP (9.6 g) was then added and ultrasonicated for 30 min, after which 2.6784 g of Zn(NO)3•6H2O was added to the supernatant and ultrasonicated for 30 min. Then, 2.9568 g of 2-methyl-imidazole was weighed into a separate beaker and dissolved in 18 mL of methanol ultrasonicated for 30 min. The 2-methyl-imidazole solution was added dropwise to the former solution, then mechanically stirred for 6 h, and separated magnetically to obtain the product. The product was washed three times with methanol, twice with anhydrous ethanol, twice with distilled water and once with anhydrous ethanol then dried for further use.

2.2.3. Preparation of ZnFe2O4@ZIF-8@ZnS (ZZZ)

Four hundred milligrams of ZZ were dissolved in 100 mL of distilled water and ultrasonicated for 20 min, after which 10 ml of Na2S•9H2O (0.01 mol/L) was added and stirred mechanically for 1 h, and the product was separated magnetically. The product was washed four times with distilled water and once with absolute ethanol, then dried for further use.

2.2.4. Preparation of ZnFe2O4@ZnS/Cu2S (ZZC)

Four hundred milligrams of ZZ were dissolved in 150 mL of methanol and sonicated for 20 min. This was followed by the addition of 40 mL of Cu(NO3)2•3H2O (0.2 mol/L) (anhydrous ethanol was used as the solvent), and the product was obtained by refluxing the product magnetically at 60 °C for 10 h. The product was washed three times with anhydrous ethanol, three times with distilled water, and dried to obtain ZnFe2O4@ZIF-8@ZnS/Cu2S (ZZZC). The final product was calcined at 300 °C for 2 h.

2.3. Characterization

The microscopic morphology of the nanomaterials was analyzed by transmission electron microscopy (TEM) using a FEITecnai Model G2F20 instrument (FEI, The Netherlands), setting the accelerating voltage to 200 kV and the maximum magnification to 80000 x. The dried samples

were characterized by X-ray diffraction (XRD) (D8 ADVANCE, BRUKER, Germany) using Ka rays with Cu targets, an operating voltage of 40 kV, operating current of 40 mA, and scanning 2θ angle 10°□90° in 0.017°/s steps. The valence states of the elements present on the surface of the materials were analyzed using X-ray photoelectron spectroscopy (XPS, Kratos, AXIS Supra, Japan); the composition, type, and content of the elements in the prepared samples were analyzed using an energy spectrometer (JEM-F200 (HRP)), and the characteristic functional groups were detected by Fourier-transform infrared spectroscopy (VERTEX 70, Bruker, Germany).

2.4. Bacteriostatic efficacy

LB solid medium was prepared using a specific ratio and autoclaved at 121°C for 40 min (LDZF-75L, Shanghai Shen'an Medical Equipment Factory). Under aseptic conditions, single colonies of the cultured bacteria were selected and placed in test tubes containing 5 mL of culture medium. The tubes were then incubated at 37°C with constant temperature and agitation for 12 h to obtain the test strains [10]. The strains were stored in a refrigerator for further use.

2.4.1. Minimum Inhibitory Concentration (MIC)

The minimum inhibitory concentration of ZZC was determined using the test tube twofold dilution method. Initially, the three test bacteria were diluted to a suspension of 1.5×108 CFU/mL. Ten sterile test tubes were prepared and numbered sequentially. Subsequently, 5 mL of the liquid culture solution and 10 μL of the suspension solution were added to each tube. The ZZC was added to 2-10 tubes, configured to a concentration of 10, 20, 30, 40, 50, 60, 70, 80and90 μg/mL of solution. Test tube No. 1 was designated as the control group. Subsequently, all test tubes were incubated in a constant temperature oscillating shaker at 30°C for 12 h. The incubation was carried out at a constant temperature of 30°C. The turbidimetric method was employed to measure the supernatant of the tubes in order, from the lowest to the highest concentration, and the BD values were recorded in three parallel sets of experiments.

2.4.2. Filter paper sheet-diffusion experiment

The filter paper diffusion method was used to characterize the bacteriostatic properties of ZZC. Solutions of ZZ and ZZC with concentrations of 50, 100, 200 and 400 μg/mL were prepared in sterile deionized water. The cultured bacterial solution was diluted to 4.5×108 colony-forming units (CFU)/mL with sterile water, applied evenly on the solid medium, and 8 μL of different materials were added dropwise on a 6 mm diameter filter paper sheet. Zinc dicentaenide (zineb) and Bordeaux solution were used as references to assess the bacteriostatic efficiency of ZZC. Experiments were conducted three times in parallel and the results were observed after 12 h of incubation in an incubator at a constant temperature of 37°C.

2.4.3. Colony counting

E. coli, S. aureus and T-Salmonella were used as the test bacteria, and the antibacterial efficiency of ZZC was quantitatively assessed by the colony counting method. A specific amount of ZZC was added to 1.5× 108 CFU/mL suspensions of the three test bacteria. The concentration of the material was 200 μg/mL. The mixture was separated using a magnet. Then, 10 μL of the resulting supernatant was absorbed and evenly spread on LB solid medium using an inoculation ring. The contact times of ZZC with the tested bacterial solution were 0, 5, 10, 20, 40 and 80 min, respectively, and it was incubated in a constant temperature incubator at 37°C for 18 h. Colony numbers were counted and the inhibition rate was calculated by applying formula (1):

$$A = \frac{B - C}{B} \times 100\%$$

Where, A indicates the inhibition efficiency, B is the number of colonies in the control group, and C is the number of colonies resulting from inhibition of the material at different inhibition.

2.5. Analysis of the mechanism of bacterial inhibition

2.5.1. Propidium iodide (PI) staining

The fluorescent dye propidium iodide (PI) can cross the cell membrane of damaged cells to stain double-stranded DNA within the bacterium [11]. In a sterile environment, the test bacteria (E. coli, S. aureus, T-Salmonella) were diluted in sterile deionized water to 1.5 × 108 CFU/mL, with the test bacterial suspension serving as the control group. Eight microliters of ZZC (10 mg/mL) and 400 μL of the test bacterial suspensions were mixed well, forming the experimental group. The materials were incubated at 25°C with shaking for 12 h. After magnetic separation, 300 μL of the supernatant was aspirated and 15 μL of PI was added for staining, then left for 10 minutes in the dark. The sample was then washed three times with phosphate-buffered saline (PBS, pH 6, 0.2 mol/L) and examined under an IX73 inverted fluorescence microscope (Olympus, Japan).

2.5.2. Determination of Zeta potential

A Zeta Potential analyzer was utilized to measure the Zeta potential of the ZZC composites against the three test bacteria (E. coli, S. aureus, T-Salmonella) with different reaction times. The concentrations of bacteria after overnight activation were 1.05×109 CFU/mL, and the Zeta potential was measured as the control group. The three test bacteria were diluted and mixed with the ZZC nanocomposites at a concentration of 200 μg/mL. The mixture was left to stand for 5 and 40 min before magnetic separation. The charge on the bacterial surface was

Journal of Environmental And Sciences (ISSN 2836-2551)

determined in the supernatant, and the data were recorded as an average of three repetitions.

2.5.3. Evaluation of cytoplasmic leakage

The leakage of bacterial contents into the solution was analyzed. Once the cell membrane of a bacterium is disrupted, the cellular endosolutes will be released into the solution and can be detected by measuring the absorbance of the solution at 260 nm using a UV-visible spectrophotometer [12]; this was used to evaluate the bacteriostatic mechanism of ZZC. After overnight growth and activation, the three test bacteria (E. coli, S. aureus and T-Salmonella) were diluted to 1.5×108 CFU/mL. Four milliliters of the bacterial solutions were placed in 5 mL centrifuge tube as the controls, while ZZC nanocomposites were added to the remaining suspensions in 5 mL centrifuge tubes to concentrations of 10 mg/mL, representing the experimental samples. The mixtures were incubated for 48 h at 25°C at room temperature with shaking, after which they were centrifuged (15000 rpm, 10 min) and the absorbances at 260 nm were measured using a UV-visible spectrophotometer, and the data were recorded and analyzed for leakage of bacterial cytoplasmic materials in three parallel groups.

2.5.4 Evaluation of ion leakage

Inductively coupled plasma mass spectrometry (ICP-MS) was used to detect the leakage of K+, Ca2+and Mg2+ ions in the bacteria to investigate the mechanism of bacterial inhibition. In the aseptic operating table, the three test bacteria were diluted according to the concentration in 2.5.2, and 3 mL of bacterial solution was added with ZZC nanocomposite (200 μg/mL) as the experimental group, and the three test bacteria were the control group. The bacterial solution of the experimental group was shaken at a constant temperature for 12 h, followed by centrifugation (15000 r/min, 10 min), and the precipitated colonies at the bottom were dissolved in aqua regia, subjected to ablation and acid-acid-driving treatments, and then cooled down to be tested for ion leakage using the instrument (three groups were tested in parallel).

2.6. Biocompatibility

Biocompatibility was assessed using the human mammary epithelial cell line MCF-7. The cells were plated in 96-well plates at a density of 1500 cells per well in medium containing 10% fetal bovine serum, and 1% penicillin and streptomycin. The cells were incubated at 37°C, saturated humidity, 5% CO2 and 95% air. The culture supernatants were then removed and 20 μL of nano-ZZC composites of different concentrations were added to each well and incubated under the same conditions for 24 h. Cell viability was assessed by the addition of 20 μL of MTT solution (10 mg/mL in PBS) with incubation for 4 h. The supernatant was removed and 100 μL of a methanolic lysing solution of dimethyl sulfoxide (DMSO) was added to dissolve the MTT crystals and incubated for 12 h. Absorbances at 630 nm were measured using a spectrophotometer and the toxicity of the material to the cells was assessed [13].

3. RESULTS AND DISCUSSION

3.1 Characterization of nano-ZZC composites

3.1.1. Analysis of ZZC morphology and elemental composition

Fig. 1 shows the flow chart of the preparation of ZZC. The nanocomposite was prepared by solvothermal reaction of magnetic ZnFe2O4 particles using FeCl3•6H2O and ZnCl2 as the raw materials, sodium acetate (NaAC) and Na3Cit as stabilizers, and ethylene glycol as a reductant. After preparation of the magnetic ZnFe2O4 particles, the surface was self-assembled with ZIF-8 with the ZnFe2O4 nucleus and the Zn2+ coordinated to 2-methylimidazole, after which the nano-ZZC composite was obtained by sulfurization and calcining using a chemical etching method. Table 1 shows the different nanocomposites and their abbreviated names.

Table1. Nanocomposites & Abbreviations

Nanocomposites	Abbreviations
ZnFe2O4@ZIF-8	ZZ
ZnFe2O4@ZIF-8@ZnS	ZZZ
ZnFe2O4@ZIF-8@ZnS/CuS	ZZZC
ZnFe2O4@ZnS/Cu2S	ZZC

Journal of Environmental And Sciences (ISSN 2836-2551)

Figure 1



Fig. 1. Schematic showing the synthesis of the nano- ZZC complexes.

Fig. 2(a-b) shows the TEM images of ZnFe2O4 and ZZC, as well as the particle size distributions. It can be seen from Fig. 2(a) that the monodispersed ZnFe2O4 NPs are spherical with an average particle size of 82.6±0.05 nm. Fig. S1 shows the uncalcined nanocomposites(ZZZC). The TEM images of the core-shell type ZZC are shown in Fig. 2(b); these had an average particle size of about 86.38±0.05 nm, which was slightly increased compared to the average particle size of ZnFe2O4 nanoparticles, indicating the loading of Cu2S on its surface. The black dots on the surface are due to the high-temperature calcination that produces the carbon elements adhering to the material surface. The HRTEM images of the ZZC are shown in Fig. 2(c), and the values of the d-spacing between the layers are 0.2995 nm and 0.255 nm correspond to the (220) and (311) crystal surfaces of spinel ferrite [14, 15]. To further investigate the elemental composition of the surfaces, EDS element mapping (Fig. 2(d-i)) and EDS energy spectra of ZZC composites (Fig. S2(a)) was performed, with the images of the nano-ZZC composites showing that the major elements within the composites included O, Fe, Zn, Cu and S, with atomic contents of 66.87%, 19.73%, 6.24%, 1.75% and 0.33%, respectively (Fig. S2(b)). In addition, the dark-field EDS elemental distribution demonstrated that O, Fe, Zn, Cu and S atoms were uniformly distributed in the shell layer.

Journal of Environmental And Sciences (ISSN 2836-2551)

Figure 2

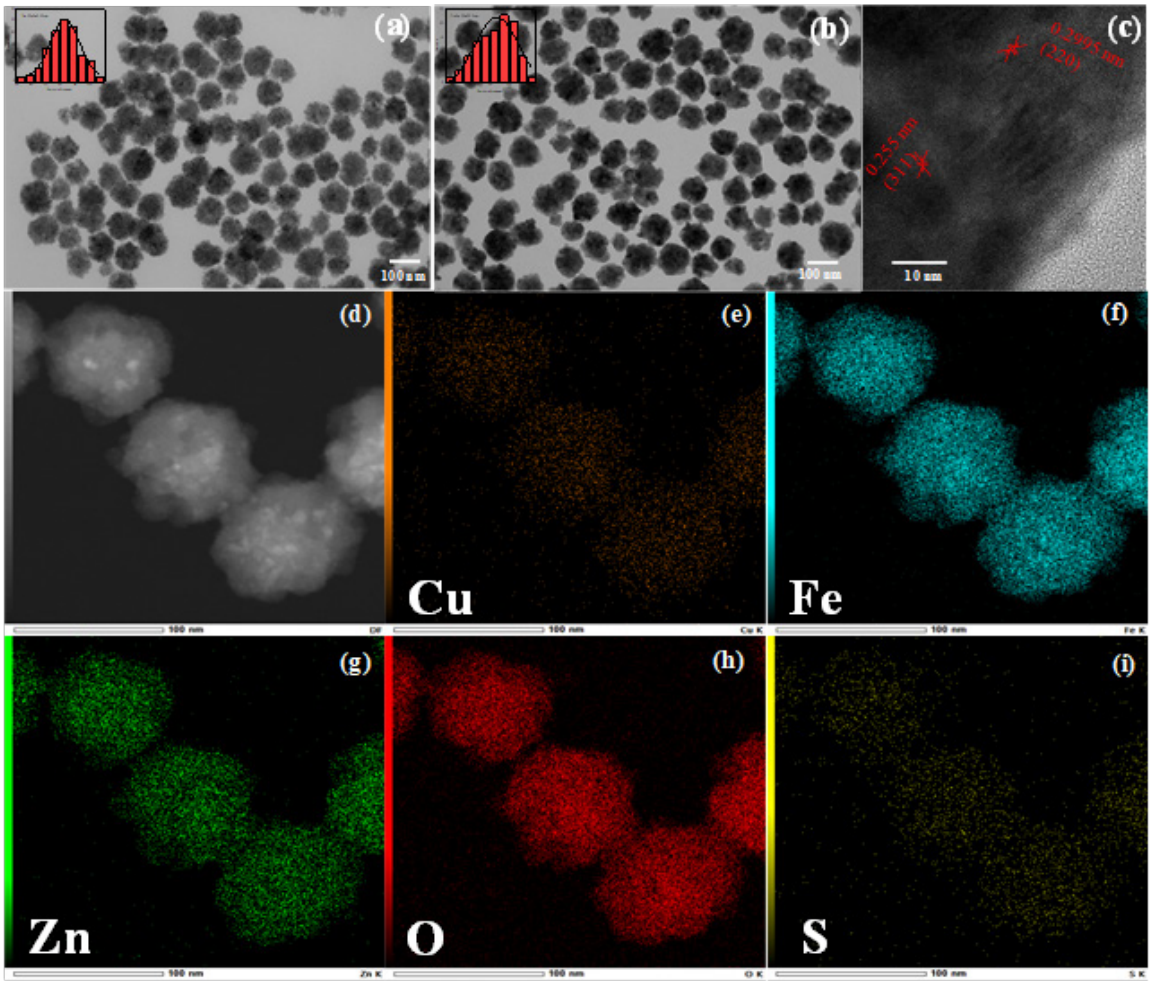


Fig. 2. TEM image of ZnFe2O4 (a) and ZZC composites (b). HRTEM of nano-ZZC composites (c). Images of EDS element mapping of nano-ZZC composites (d, e, f, g, h, i)

3.1.2. Analysis of ZZC crystal type and elemental valence

For further verification of the surface elements, analyses of the physical phase composition and electronic valence states of the prepared nano-ZZC composites were performed using X-ray photoelectron spectroscopy and X-ray diffraction. Fig. 3(a) shows the full-scan XPS spectra of the nanocomposites, from which it can be seen that the characteristic peaks of the elements Cu, Zn, Fe, C, O and S are present, as shown in Fig. 3(b). The two characteristic peaks located at 952.8 and 932.6 eV represent the binding energies of Cu2p1/2 and Cu2p3/2, respectively, which corresponds to the characteristic peaks of Cu+ in Cu2S, Cu2+ in CuS Cu2p3/2 and Cu2p1/2 binding energies [16], and satellite characteristic peaks at 961.7 and 942.0 for Cu2+, which correspond to the Cu2+ state [17, 18].Fig. 3(c) shows the binding energies for Zn, with 1020.8 eV and 1043.8 eV attributed to the binding energies of Zn2p3/2 and Zn2p1/2, respectively The fitted peak at 1044.9 eV is attributed to the Zn-O bond in ZnO, and the fitted peak at 1022.0 eV is attributed to the Zn2p response in ZnFe2O4 which suggests that Zn is present in the oxide in the Zn2+ state [19]. Fig. 3(d) shows the characteristic peaks of Fe2p, with the binding energies at 711.4 eV and 725.2 eV attributed to Fe2p3/2 and Fe2p1/2, respectively [20], together with two vibrational satellite peaks at 718.6 eV and 709.9 eV, demonstrating that Fe is present in ZnFe2O4 in both the Fe3+ and Fe2+ forms. In the C1s spectrum shown in Fig. 3(e), elemental C is split into two peaks at 287.30 and 284.64 eV, indicating the presence of two types of carbon bonding, with the peak at 287.3 eV attributed to C-O and the peak at 284.6 eV to C-C. The O1s spectra displayed in Fig. 3(f) illustrate that the characteristic signals of C=O and C-O-C functional groups, are associated with the peaks at 533.5 and 531.1 eV, respectively [21]. The lattice oxygens (M-O, referred to as OLatt) in ZnFe2O4 consist of Zn-O and Fe-O bonds, as well as adsorbed oxygens or surface hydroxyl species of the catalyst (referred to as Oads) [22]. The peak at 161.2 eV in Fig. 3(g) is attributed to S2p1/2 , with elemental S present in the form of S2- [23].

Journal of Environmental And Sciences (ISSN 2836-2551)

The XRD spectra are shown in Fig. 3(h). The peaks at 29.9°, 35.3°, 42.9°, 56.6°, and 62.1° correspond to the (220), (311), (400), (511) and (440) planes of ZnFe2O4, which are in general agreement with the standardized spectral position (JCPDS22-1012) of ZnFe2O4 [24]. The diffraction peaks of the XRD spectra of ZZ nanocomposites showed significant diffraction peaks at 2θ= 7.3°, 10.5°, 12.8°, 14.8°, 16.5° and 18.1° compared to ZnFe2O4, which correspond to (011), (002), (112), (022), (013) and (014), respectively, especially a very long and sharp characteristic peak at 2θ = 7.3°, indicating that the high purity and crystallinity of the incorporated ZIF-8 crystals [25]. ZZ showed significantly improved crystallinity due to the increase in the Zn2+ content, and the lack of Cu detection in the ZZC characteristic peaks may have resulted in a Cu2S content below the limit of detection. The XRD spectra of ZZC after calcination showed slightly modified crystallinity due to the disappearance of some peaks caused by the carbonization of the material surface covering the internal crystalline surface.

Fig. 3(i) shows the FT-IR spectra of ZnFe2O4, ZZ, ZZIF, ZZZC and ZZC, and it can be seen that there are obvious infrared vibrational absorption peaks of ZnFe2O4 at 454 cm-1 and 569 cm-1. These absorption peaks are characteristic of metal-oxygen bonding in the ZnFe2O4 structure [26], with the former presenting the telescopic vibration peak of Zn2+-O2- at the octahedral position formed by O2- ions, and the latter the telescopic vibration peak of Fe3+-O2- at the tetrahedral position formed by O2- ions, indicating the presence of Zn-O and Fe-O bonding in the sample. Compared to ZnFe2O4, the absorption peaks of ZZ at 2927 cm-1 and 3134 cm-1 are attributed to the stretching vibrations of the saturated hydrocarbon C-H(CH3) and unsaturated hydrocarbon C-H of 2-methylimidazolium [27], respectively, indicating that 2-methylimidazolium plays the role of organic ligands in the nanocomposites. The peak at 1581 cm-1 represents C=N stretching vibrations, with C-N stretching vibrations at 1146 cm-1 and 995 cm-1; the peak at 1306 cm-1 is attributed to imidazolium ring vibration, and the peak at 418 cm-1 is caused by Zn-N bond stretching vibration. These findings demonstrate the successful encapsulation of ZIF-8 in ZnFe2O4. The FT-IR spectra of ZZ showed no significant changes in the peak positions compared to ZZ. The characteristic peaks of C=N in ZZZC have shifted to the left, suggesting that there may be an interaction between copper and nitrogen [28].

Figure 3

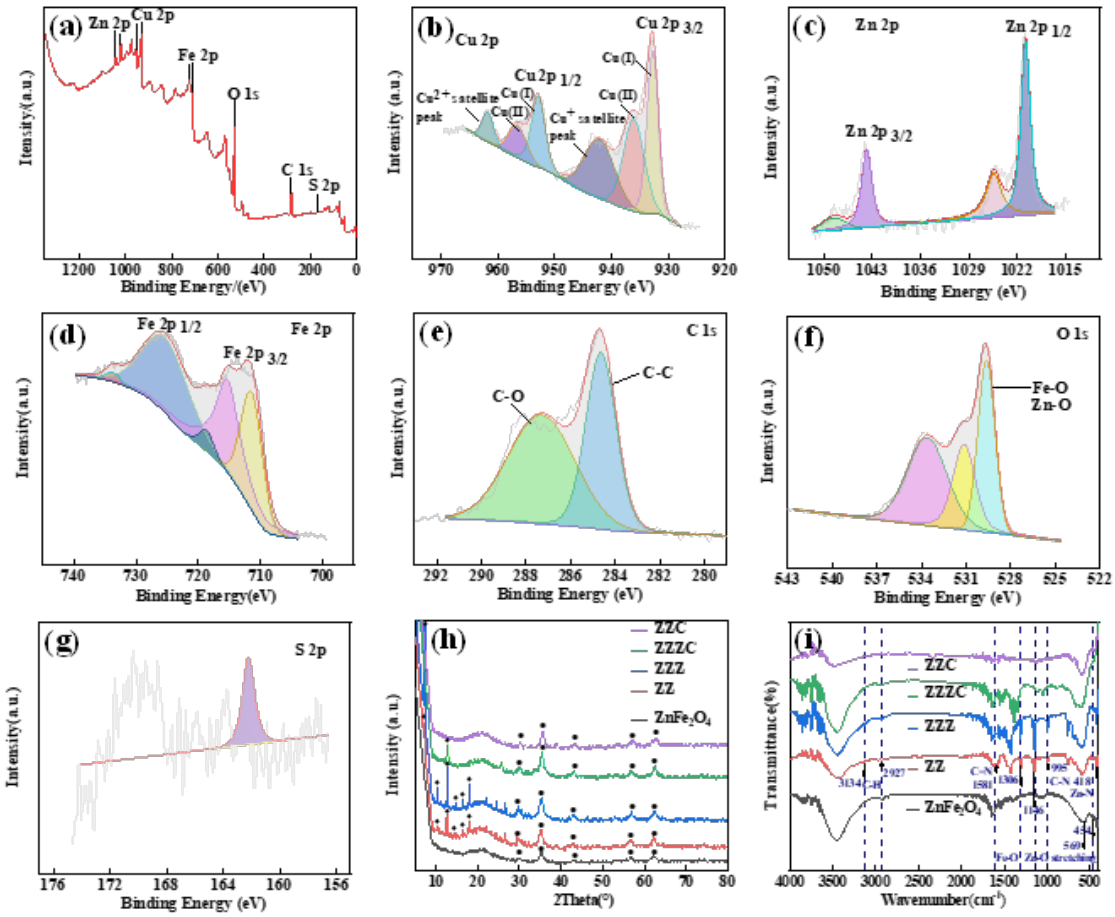


Fig. 3. Full-scan XPS spectra of the nanocomposites (a). XPS spectra of Cu2p (b), Zn2p (c), Fe2p (d), C1s (e), O1s (f) and S2p (g) in nano-ZZC composites. XRD pattern of nano-ZZC composites (h). FT-IR spectra of nano-ZZC composites (i).

Journal of Environmental And Sciences (ISSN 2836-2551)

3.2 Bacteriostatic efficacy of nano-ZZC composites

3.2.1 MIC

The results of the MIC tests for different concentrations of ZZC on the three test bacteria, E. coli, S. aureus and T-Salmonella, are presented in Fig. S3. E. coli was successfully removed from test tube No. 6, at which time the value of the turbidimeter test was 0.25 (Table 2), and that of the control group No. 1 was 5.73, the concentration of the bacterial solution subsequently decreased by approximately 96%. This indicated that the MIC value of the composites on E. coli was 50 μg/mL, and similarly for S. aureus and T-Salmonella, the MIC values were 60 and 80 μg/mL, respectively. The inhibitory effect of ZZC on the three tested bacteria was observed to be greatest against E. coli, with a lesser effect observed against S. aureus and T-Salmonella.

Table 2. MIC values of nano-ZZC on E. coli, S. aureus, T-Salmonella

	Material / Material concentration gradients c(μg/mL) / BD (1×108 CFU/mL)									
	ZZC									
Bacteria	0	10	20	30	40	50	60	70	80	90
E. coli	5.73	4.97	3.84	2.65	1.98	0.25	0.20	0.19	0.17	0.16
S. aureus	6.24	5.87	4.26	3.97	3.02	2.66	0.21	0.19	0.18	0.15
T-Salmonella	4.59	4.03	3.63	3.22	2.87	2.45	2.06	1.64	0.27	0.18

3.2.2 Filter paper sheet diffusion method

The bacteriostatic effects of ZZC nanocomposites against E. coli, S. aureus and T-Salmonella were determined by the filter paper sheet diffusion method. Fig. 4(a-c). shows the bacteriostatic properties of the different materials (ZZ, ZZC) at different concentrations against E. coli, S. aureus and T-Salmonella. Among them, I and II (zineb and Bordeaux solution, respectively) were used as controls, and an absence of inhibition circles is clearly visible in all four samples when the concentration of the three materials was 50 μg/mL. From Fig. 4(d-f), it can be seen that the bacteriostatic effects of the materials increased in correspondence with their concentrations, while ZZ did not show bacteriostatic activity, due to the outer coating structure of the material preventing the release of ZnFe2O4. At concentrations of 100, 200 and 400 μg/mL, ZZC produced larger inhibitory circles compared with zineb and Bordeaux solution at the same concentration. The inhibition efficiency of the nanocomposites against E. coli, S. aureus and T-Salmonella was increased by 2.18, 1.62 and 1.31 times, respectively, compared with the control Bordeaux solution at a concentration of 400 μg/mL. The composites showed 2.79, 1.44 and 1.31 times higher inhibition efficiency against E. coli, S. aureus and T-Salmonella, respectively, compared to zineb. In conclusion, the bacteriostatic properties of the composites were significantly stronger than those of the commercially available inorganic bacteriostatic compounds. Among them, the ZZC nanocomposites showed stronger inhibitory performance against E. coli than against S. aureus and T-Salmonella, which demonstrated the higher inhibitory activity of the nanocomposites against the Gram-negative bacterium E. coli.

Journal of Environmental And Sciences (ISSN 2836-2551)

Figure 4

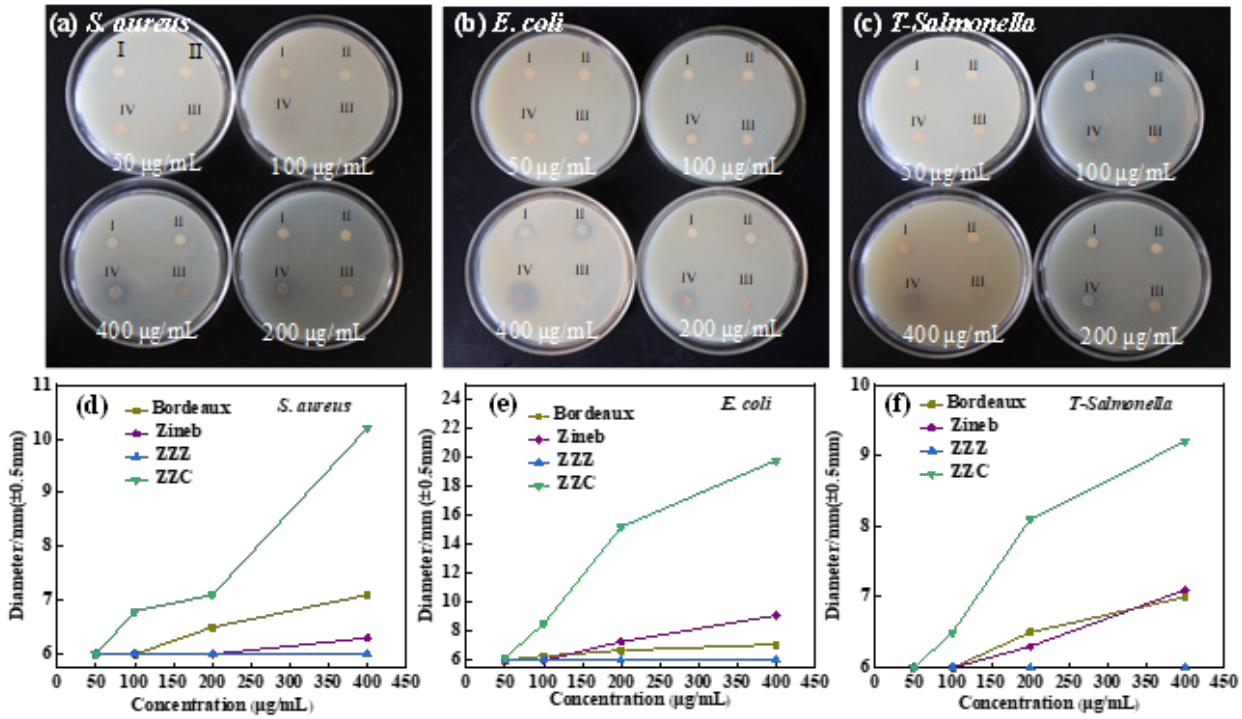


Fig. 4. Results of filter paper diffusion of different concentrations of zineb, Bordeaux solution, and ZZ and nano-ZZC composites against S. aureus (a), E. coli (b) and T-Salmonella (c). Curves showing the diameters of the bacteriostatic circles of different materials with different concentrations against S. aureus(d), E. coli(e) and T-Salmonella(f).

3.2.3 Colony-counting method

To further investigate the antibacterial properties of ZZC nanocomposites, we analyzed the antibacterial efficacy of the composites at a concentration of 200 μg/mL after mixing with S. aureus (Fig. 5(a)), E. coli (Fig. 5(b)), and T-Salmonella (Fig. 5(c)). The colony-counting method was utilized to determine antibacterial activity at 0, 5, 10, 20, 40 and 80 min. (□) indicates the control group and as can be seen from the figure, increased mixing time was associated with greater inhibition of the growth of the three test bacteria, and the inhibitory effects of the nanocomposites on the three test bacteria, E. coli, S. aureus and T-Salmonella, were obviously enhanced. Fig. 5(d) shows the number of colonies observed after mixing the three test bacteria with the material for different times, and Fig. 5(e) shows the inhibition rate of ZZC nanocomposites against the bacteria demonstrating inhibition rates of 69.1% (±0.1%) after 5 min incubation with E. coli, S. aureus and T-Salmonella, increasing after 10 min to 97.3% in E. coli, while the inhibition of S. aureus and T-Salmonella reached 94.9% and 82.6%, respectively. By 40 min, the rate of inhibition of all three bacteria was over 99%.

Journal of Environmental And Sciences (ISSN 2836-2551)

Figure 5

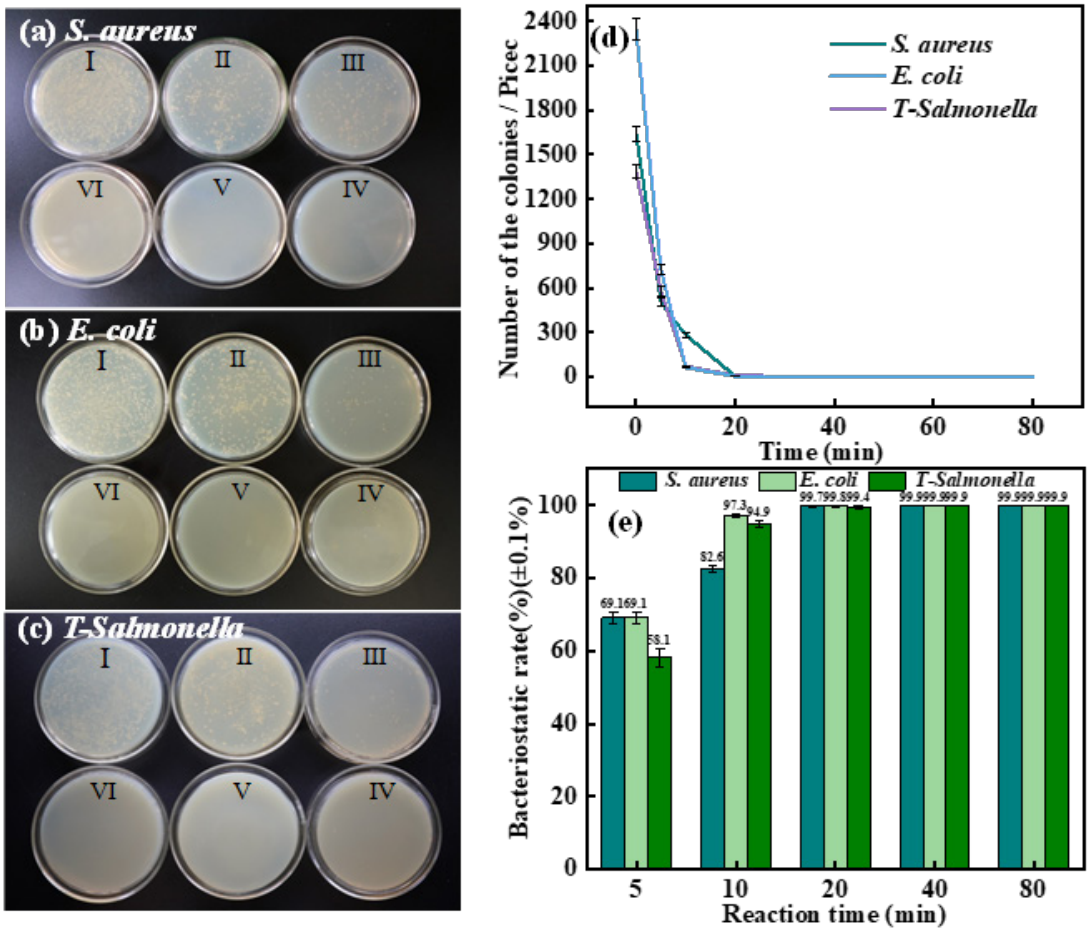


Fig. 5. Colony-counting results for S. aureus (a), E. coli (b) and T-Salmonella (c) with nano-ZZC composites at a concentration of 200 μg/mL. (d) Colony numbers at different times after treatment of the three test bacteria with nano-ZZC composites. (e) Bacteriostatic rates of nano-ZZC composites against the three test bacteria at different times.

3.3 Mechanism of bacterial inhibition by nano-ZnFe2O4@ZnS/Cu2S composites

3.3.1. Analysis of the results of PI staining

The fluorescent dye PI stains the DNA of dead cells, resulting in the nuclei of dead cells emitting red fluorescence when examined under fluorescence microscopy [11, 29]. As can be seen in Fig. 6(a-c), a few bacteria in the blank control group of the pure bacterial suspensions of E. coli, S. aureus and T-Salmonella showed red fluorescent dots after PI staining, indicating low numbers of dead bacteria. However, after incubation of the ZZC composite with the test bacteria for 12 h, all three bacteria showed greater numbers of red fluorescent dots, with the most seen for E. coli (Fig. 6(e)), indicating that the composite caused the most serious membrane damage to E. coli, followed by S. aureus (Fig. 6(d)), while the effect was weaker for the drug-resistant bacterium T-Salmonella (Fig. 6(f)). The experimental results showed that the nano-ZZC composite could effectively damage the bacterial cell membrane.

Journal of Environmental And Sciences (ISSN 2836-2551)

Figure 6

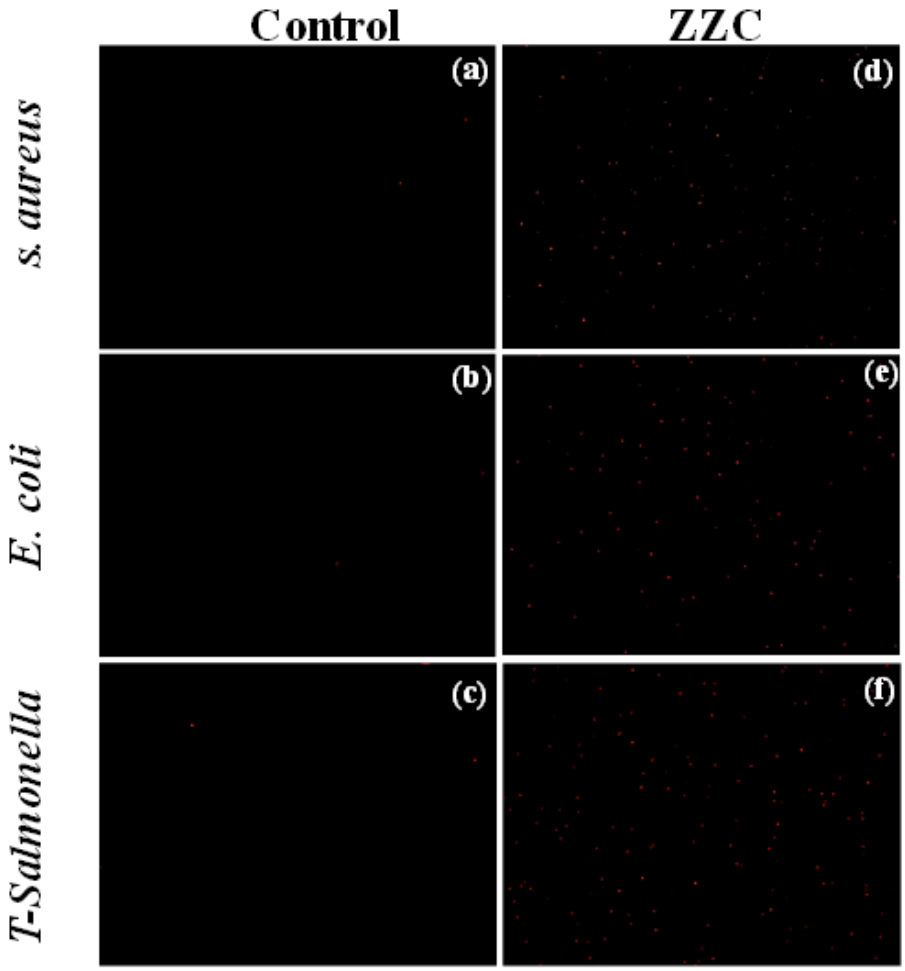


Fig. 6. Three test bacteria not treated with nano-ZZC (a-c). Representative fluorescence images of bacterial cells after 12 h of treatment. Dead S. aureus (d), E. coli (e) and T-Salmonella (f), shown by PI staining.

3.3.2. Zeta potential analysis

Zeta potential measurements can effectively assess the degree of mutual repulsion or attraction between nano-materials within biological systems and the environment, as well as reveal the surface charge distribution of cell membranes [30]. Fig. 7(a) demonstrates the impact of mixing 200 μg/mL of nano-ZZC composite with E. coli, S. aureus and T-Salmonella for 5 and 40 min on the Zeta potential values of the bacterial cell membranes. Using the Zeta potential values of pure E. coli, S. aureus and T-Salmonella as the controls, the values for the surface potentials of the three tested bacteria were -14.50, -16.02 and -14.67 mV, respectively. Since lipopolysaccharides and lipoproteins in the bacterial cell wall contain negatively charged reactive groups such as -OH, -COOH, -CONH2 and -NH2. The figure shows that the surface potentials of nano-ZZC composites after mixing with E. coli, S. aureus and T-Salmonella for 5 min were -10.75 -12.62 and -11.45 mV, respectively. Subsequently, after 40 min, the surface potentials of the three bacteria were -3.76, -5.89 and -5.92 mV, respectively. The nano-ZZC can effectively neutralise the surface charge of bacterial cell walls and have a more pronounced effect on E. coli.

3.3.3 Analysis of the results of Cytoplasmic leakage

Cytoplasmic leakage was used for further investigation of the bacteriostatic mechanism of the nano-ZZC composites against the bacteria. Damage to microbial cell membranes leads to the release of intracellular components, including DNA, RNA, plasmids, and other biomolecules, into the surrounding environment. The absorption peaks of the released materials were measured at 260 nm using a UV-visible spectrophotometer. The outcomes are depicted in Fig 7. Compared to the control group, the absorbance at 260 nm of S. aureus (Fig. 7(b)), E. coli (Fig. 7(c)) and T-Salmonella (Fig. 7(d)) demonstrated a notable

Journal of Environmental And Sciences (ISSN 2836-2551)

increase in the absorbance at 260 nm after exposure to the nano-ZZC composite material. This significant increase is indicative of the substantial leakage of the bacterial cellular contents.

Figure 7

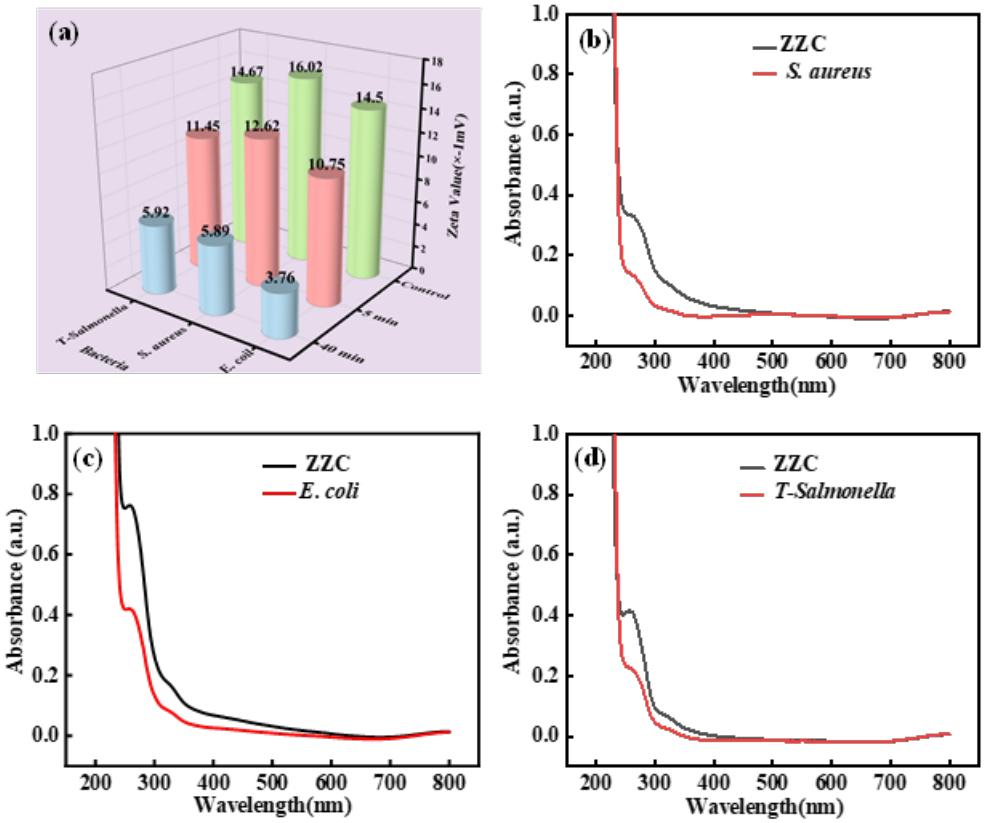


Fig. 7. Zeta potentials of 200 μg/mL nano-ZZC composites mixed with S. aureus, E. coli and T- Salmonella for 5 and 40 min (a). Toxicity analysis of the composites (b). Cytoplasmic leakage of S. aureus (c), E. coli (d) and T-Salmonella (e) after treatment with the nanocomposites.

3.3.4 Analysis of the results of ion leakage

Damage to the bacterial cell membrane leads to leakage of intracellular ions, which results in metabolic disorders [31]. In this experiment, the degree of change in cell membrane permeability of three test bacteria, E. coli, S. aureus and T-Salmonella, by ZZC nanocomposites was further evaluated by determining the leakage of K+, Ca2+, and Mg2+ in the bacteria. Fig 8(a-c) shows the results of the effect of composites on the leakage of intracellular K+, Ca2+, and Mg2+ of the three test bacteria, where the concentrations of intracellular K+ in E. coli, S. aureus, and T-Salmonella in the control group were 1.68, 2.26, and 1.66 mg/L, respectively; the concentrations of Ca2+ were 1.49, 1.27, and 1.10 mg/L, respectively and the concentrations of Mg2+ were 0.97, 0.82 and 0.72 mg/L, respectively, indicating that the bacterial cells maintained their own normal ion channels. After a period of time of ZZC action, the concentrations of intracellular K+ in E. coli, S. aureus and T-Salmonella were 0.34, 0.84 and 0.63 mg/L, respectively, and those of Ca2+ were 0.62, 0.65 and 0.59 mg/L, and the concentrations of Mg2+ were 0.48, 0.49 and 0.45 mg/L, respectively, which were significantly lower than those of the control. ZZC materials can effectively destroy the normal physiological functions of bacteria, resulting in the disruption of their ion channels.

3.4 Cytotoxicity result analysis

Biocompatibility is critical for nanomaterials to be applied in biomed-icine [3, 31].Therefore, the biocompatibility of the nano-ZZC composites was evaluated by comparing the toxicities of nano-ZZC composites and GDC-0941 anticancer composites on MCF-7 human mammary epithelial cells, which were cultured with different drugs for 24 h. The results are shown in Fig. 8(d). The IC50 values, compared with the negative control group, of GDC-0941 and ZnFe2O4@ZnS/Cu2S were 308.18 and 280.52 (±0.05) μg/mL, respectively, which showed no statistically significant difference. It can be seen that the biocompatibility of

Journal of Environmental And Sciences (ISSN 2836-2551)

the ZZC nanocomposites is similar to that of the commercially available anticancer drug GDC-0941, demonstrating the good biocompatibility of the nanocomposites.

Figure 8

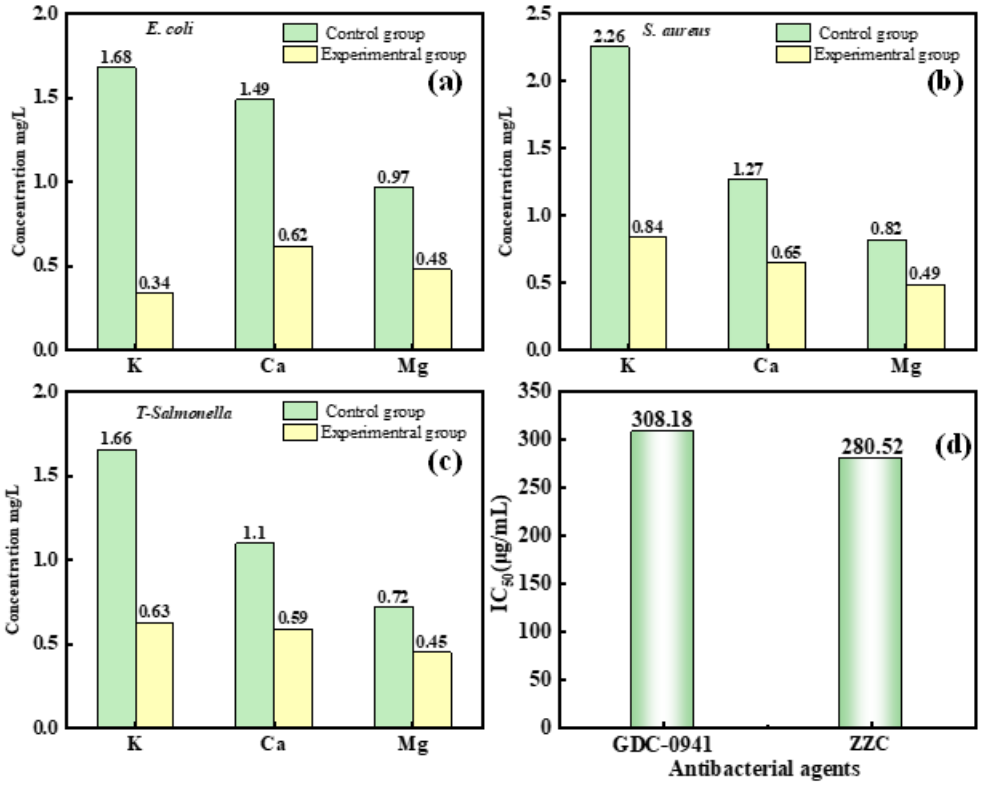


Fig. 8. The results of Ion leakage of E. coli (a), S. aureus (b) and T-Salmonella (c). Toxicity analysis of the composites (d).

3.5 Mechanism of bacterial inhibition by ZZC nanocomposites

In this study, we investigated the interactions between nano-ZZC composites and Gram-negative and Gram-positive bacteria using Zeta potential analysis, PI staining, and analysis of cytoplasmic leakage and proposed a possible mechanism of bacterial inhibition (Fig. 9). E. coli cell walls are approximately 10-15 nm and consist of phospholipids, lipopolysaccharides and proteins that form the outer membrane [32, 33], whereas the cell wall of S. aureus consists of a thick peptidoglycan (PGN) layer (20-80 nm), which is thicker and more compact, and interspersed with a large amount of phosphoglycolic acid [34, 35]. The layer is surrounded by anionic glycopolymers, resulting in the cell walls having a negative potential difference due to the presence of -OH, -NH2, -COOH, -CONH2 and other groups. Cu2+, Zn2+and Fe3+ ions released from the ZZC nanocomposites during the interaction with the bacteria can be electrostatically adsorbed onto the cell membranes of Gram-negative bacteria, altering the secondary structures of proteins, and thus increasing the permeability of the membrane and ultimately resulting in the death of the microorganism. This is consistent with the results of the Zeta potential measurements. The ZZC nanocomposites material can cause bacterial death by disrupting the bacterial cell membrane ion channels, resulting in a massive leakage of K+□Ca2+and Mg2+ ions

Essential metal ions, such as Cu, Zn and Fe, are involved in essential cellular functions, such as the synthesis of key enzymes and electron transport processes, as well as in the structure of cell membranes and DNA [36, 37]. However, they can also have lethal effects on bacterial cells. For example, high concentrations of metal ion can negatively affect a variety of bacterial activities, such as glycolysis, transmembrane proton translocation and acid resistance, thereby prolonging the lag phase in bacterial growth [38] and triggering metal mismatches in various metal-binding proteins, leading to protein dysfunction, enzyme inactivation, or protein denaturation, all of which disrupt the equilibrium of the bacterial cell. Zn2+ and Cu2+ ions released from ZZC can bind to DNA, disrupting its helical structure and leading to the death of the bacterial cell [39]; this is consistent with the results of the PI staining. Another possible mechanism may be through the generation of reactive oxygen

Journal of Environmental And Sciences (ISSN 2836-2551)

species (ROS) through the Fenton reaction [40]. Under physiological conditions, iron exists mainly in two oxidation states, namely, the oxidized Fe3+ (trivalent iron) and the reduced Fe2+ (ferrous iron) forms. Fe2+ is easily oxidized, releasing electrons that can combine with oxygen to produce ROS [41] while combination with Zn2+ not only increases electron mobility but also causes fatal damage to bacterial pathogens. Accumulation of ROS induces oxidative stress in the cell, potentially damaging bacterial membranes, ribosomes, proteins, and DNA[43].

Figure 9

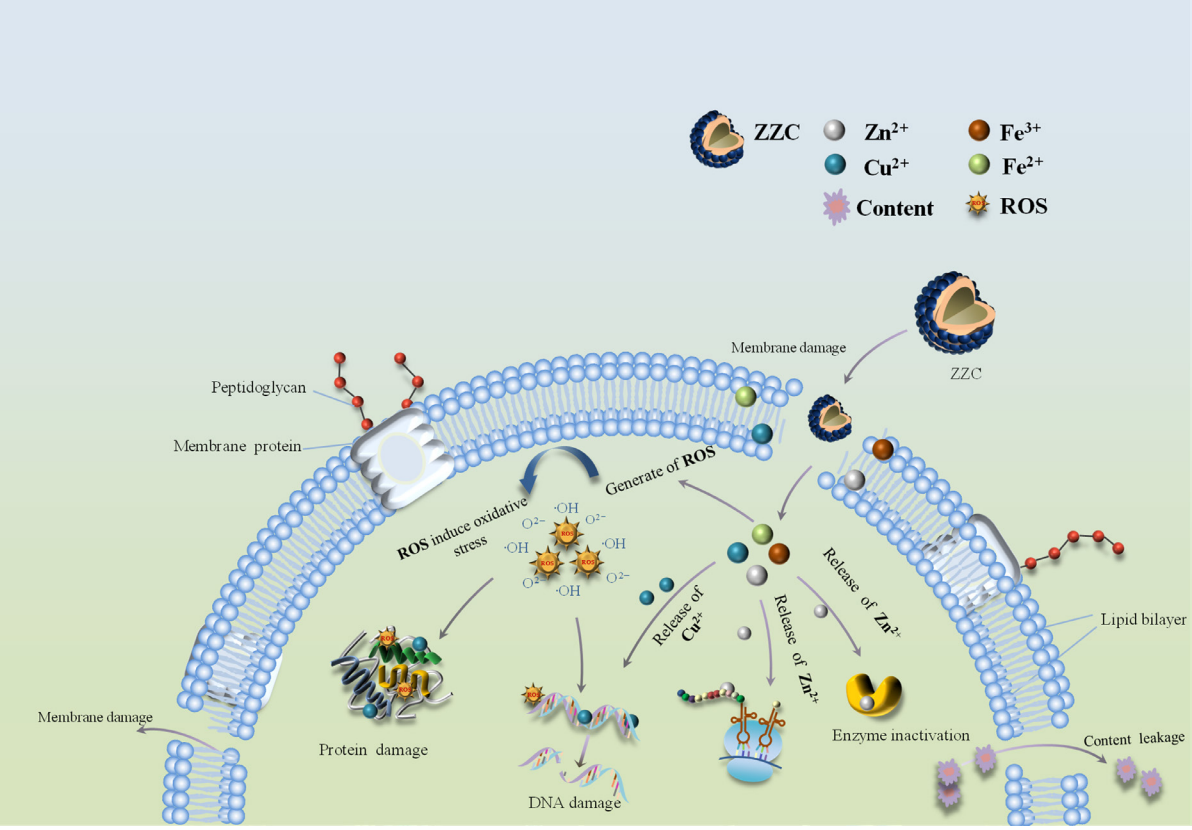


Fig. 9. Schematic depicting the bacteriostatic mechanism.

4. CONCLUSION

This study details the preparation of a new nanomaterial, ZnFe2O4, through the solvothermal method. A layer of ZIF-8 with a dodecahedral structure was used as the nucleus which was then coated with ZnFe2O4 is coated, resulting in the formation of ZZC nanocomposites via “layer-coating”. The morphology of the ZZC nanocomposites was assessed using TEM, revealing the presence of core-shell spherical nanostructures on the surface.

The study investigated the bacteriostatic effects of the composites and found that they were significantly superior to those of available agrochemicals. The MIC of the ZnFe2O4@ZnS/Cu2S against E. coli, S. aureus and T-Salmonella were 50, 60 and 80 μg/mL, respectively; At a concentration of 200 μg/mL, the composites displayed excellent antibacterial activity against E. coli, S. aureus and T-Salmonella, with inhibition rates for the three bacteria reaching 99.99% within 80 min. In vitro biological experiments demonstrated that the ZZC nanoparticles possessed substantial antibacterial efficacy and favorable biocompatibility.

Based on the results of Zeta potential measurements, PI staining and cytoplasmic and ion leakage experiments, it is hypothesized that the composite material inhibits microbial growth by releasing Zn2+, Cu2+, Fe3+, negatively charged lipoproteins, and lipopolysaccharides from the cell wall through electrostatic attraction. This causes increased permeability of the microbial cell membrane and a change in the surface structure of the cell wall. Additionally, another possible mechanism involves the production of ROS which can cause oxidative stress within the cell, causing damage to proteins and DNA. This also impacts bacterial membranes, lipids, proteins and DNA, leading to oxidative stress. In summary, ZZC demonstrated remarkable

bacteriostatic properties, providing a solid foundation for the future development of materials for medical treatments and other areas.

Data and materials availability

All data are included in the manuscript and Supporting Information are available from the corresponding authors on request.

Author Contributions

Xinli Zhou as the first author designed and synthesized nanomaterials. Huihui Chen, Jiawei Wang and Miao Wu characterized and analyzed the data of the nanomaterials. Riuling Hu, Junpeng Yang and Tinghui Qiang carried out experimental analysis of the bacteriostatic properties. Huan Mou and Xingguo Du explored the mechanism of bacterial inhibition. Fei Gao and Zhongshang Guo wrote the first draft of the manuscript, all authors commented and modified on previous versions.

Declaration of competing interest

The authors declare that they have no known competing financial interests or personal relationships that could have appeared to influence the work reported in this paper.

Acknowledgments

Foundations: Key Researchand Development Program of Key Researchand Development Program of Shaanxi (Program No.2024SF-YBXM-158), Shaanxi Province Health and Wellness Scientific Research Innovation Capacity Enhancement Project (Program No.2024PT-16) and Hanzhong Central Hospital Hospital-Level Scientific Research Fund Project (Program No.YK2417) provided financial support for this work.

REFERENCES

1. N.D. Friedman, E. Temkin, Y. Carmeli, The negative impact of antibiotic resistance, Clinical Microbiology and Infection. 22 (2016) 416-422, https://doi.org/10.1016/j.cmi.2015.12.002.

2. Q. Song, R. Zhao, T. Liu, L. Gao, C. Su, Y. Ye, S.Y. Chan, X. Liu, K. Wang, P. Li, One-step vapor deposition of fluorinated polycationic coating to fabricate antifouling and anti-infective textile against drug-resistant bacteria and viruses, Chemical Engineering Journal. 418 (2021) 129368, https://doi.org/10.1016/j.cej.2021.129368.

3. Y. Wan, J. Fang, Y. Wang, J. Sun, Y. Sun, X. Sun, M. Qi, W. Li, C. Li, Y. Zhou, Antibacterial zeolite imidazole frameworks with manganese doping for immunomodulation to accelerate infected wound healing, Advanced Healthcare Materials. 10 (2021) 2101515, https://doi.org/10.1002/adhm.202101515

4. G.V. Vimbela, S.M. Ngo, C. Fraze, L. Yang, D.A. Stout, Antibacterial properties and toxicity from metallic nanomaterials, International journal of nanomedicine. (2017) 3941-3965, https://doi.org/10.2147/IJN.S134526.

5. B. Paz-Diaz, A.R. Vazquez-Olmos, A. Almaguer-Flores, V.I. García-Pérez, R.Y. Sato-Berru, Y.C. Almanza-Arjona, V. Garibay-Febles, ZnFe2O4 and CuFe2O4 nanocrystals: synthesis, characterization, and bactericidal application, Journal of Cluster Science. 34 (2023) 111-119, https://doi.org/10.1007/s10876-021-02203-4.

6. R. Abedinpour Farahmand, F. Raouf, S. Hamedi, N. Gilani, Investigation on antibacterial activity of α-Fe2O3/ZnO nanocomposites against Gram-positive and Gram-negative bacteria, Materials Technology. 37 (2022) 2265-2275, https://doi.org/10.1080/10667857.2022.2026105.

7. M. Gharibshahian, O. Mirzaee, M. Nourbakhsh, Evaluation of superparamagnetic and biocompatible properties of mesoporous silica coated cobalt ferrite nanoparticles synthesized via microwave modified Pechini method, Journal of Magnetism and Magnetic Materials. 425 (2017) 48-56, https://doi.org/10.1016/j.jmmm.2016.10.116.

8. A. Khalid, P. Ahmad, A.I. Alharthi, S. Muhammad, M.U. Khandaker, M.R.I. Faruque, I.U. Din, M.A. Alotaibi, A. Khan, Synergistic effects of Cu-doped ZnO nanoantibiotic against Gram-positive bacterial strains, Plos one. 16 (2021) e0251082, https://doi.org/10.1371/journal.pone.0251082.

9. N. Wei, Y. Tang, Y. Li, Q. Wang, W. Zeng, D. Liang, R. Wu, Metal–organic frameworks-derived hollow octadecahedron nanocages for supercapacitors and wearable self-powered tactile stress sensor, Applied Surface Science. 599 (2022) 153822, https://doi.org/10.1016/j.apsusc.2022.153822Get rights and content.

10. J. Pu, Z. Zhang, H. Zhang, Y. Xu, B. Zhang, M. Yang, K. Li, L. Zhang, S. Xiong, N. Zhong, Efficacy of Bactericides Against Potato Common Scab Caused by Streptomyces in Yunnan, China, American Journal of Potato Research. 99 (2022) 326-335, https://doi.org/10.1007/s12230-022-09883-2.

11. H.Y. Lwin, Y. Aoki-Nonaka, A. Matsugishi, N. Takahashi, T. Hiyoshi, K. Tabeta, Soybean peptide inhibits the biofilm of periodontopathic bacteria via bactericidal activity, Archives of Oral Biology. 142 (2022) 105497, https://doi.

org/10.1016/j.archoralbio.2022.105497.

12. H.Y. Yang, C.M. Chang, Y.W. Chen, C.C. Chou, Inhibitory effect of propolis extract on the growth of Listeria monocytogenes and the mutagenicity of 4□nitroquinoline□N□oxide, Journal of the Science of Food and Agriculture. 86 (2006) 937-943, https://doi.org/10.1002/jsfa.2441.

13. X. Wang, L. Mei, M. Jin, X. Jiang, X. Li, J. Li, Y. Xu, Z. Meng, J. Zhu, F. Wu, Composite coating of graphene oxide/TiO2 nanotubes/HHC-36 antibacterial peptide construction and an exploration of its bacteriostat and osteogenesis effects, Journal of Biomedical Nanotechnology. 17 (2021) 662-676, https://doi.org/10.1166/jbn.2021.3013.

14. A. Behera, D. Kandi, S.M. Majhi, S. Martha, K. Parida, Facile synthesis of ZnFe2O4 photocatalysts for decolourization of organic dyes under solar irradiation, Beilstein journal of nanotechnology. 9 (2018) 436-446, https://doi.org/10.3762/bjnano.9.42.

15. A. Behera, S. Mansingh, K.K. Das, K. Parida, Synergistic ZnFe2O4-carbon allotropes nanocomposite photocatalyst for norfloxacin degradation and Cr (VI) reduction, Journal of colloid and interface science. 544 (2019) 96-111, https://doi.org/10.1016/j.jcis.2019.02.056.

16. J. Li, J. Ma, L. Hong, C. Yang, Prominent antibacterial effect of sub 5 nm Cu nanoparticles/MoS2 composite under visible light, Nanotechnology. 33 (2021) 075706, https://doi.org/10.1088/1361-6528/ac3577.

17. M. Yin, C.-K. Wu, Y. Lou, C. Burda, J.T. Koberstein, Y. Zhu, S. O'Brien, Copper oxide nanocrystals, Journal of the American Chemical Society. 127 (2005) 9506-9511, https://doi.org/10.1021/ja050006u.

18. S. Chawla, N. Sankarraman, J. Payer, Diagnostic spectra for XPS analysis of Cu O S H compounds, Journal of electron spectroscopy and related phenomena. 61 (1992) 1-18, https://doi.org/10.1016/0368-2048(92)80047-C.

19. Y. Jin, Q. Cui, G. Wen, Q. Wang, J. Hao, S. Wang, J. Zhang, XPS and Raman scattering studies of room temperature ferromagnetic ZnO: Cu, Journal of Physics D: Applied Physics. 42 (2009) 215007, https://doi.org/10.1088/0022-3727/42/21/215007.

20. Y. Zhou, B. Xiao, S.-Q. Liu, Z. Meng, Z.-G. Chen, C.-Y. Zou, C.-B. Liu, F. Chen, X. Zhou, Photo-Fenton degradation of ammonia via a manganese–iron double-active component catalyst of graphene–manganese ferrite under visible light, Chemical Engineering Journal. 283 (2016) 266-275, https://doi.org/10.1016/j.cej.2015.07.049.

21. M.B. Askari, P. Salarizadeh, M. Seifi, A. Di Bartolomeo, ZnFe2O4 nanorods on reduced graphene oxide as advanced supercapacitor electrodes, Journal of Alloys and Compounds. 860 (2021) 158497, https://doi.org/10.1016/j.jallcom.2020.158497.

22. Z. Wang, H. Ma, C. Zhang, J. Feng, S. Pu, Y. Ren, Y. Wang, Enhanced catalytic ozonation treatment of dibutyl phthalate enabled by porous magnetic Ag-doped ferrospinel MnFe2O4 materials: Performance and mechanism, Chemical Engineering Journal. 354 (2018) 42-52, https://doi.org/10.1016/j.cej.2018.07.177.

23. W. Liu, H. Xu, Y. Liao, Z. Quan, S. Li, S. Zhao, Z. Qu, N. Yan, Recyclable CuS sorbent with large mercury adsorption capacity in the presence of SO2 from non-ferrous metal smelting flue gas, Fuel. 235 (2019) 847-854, https://doi.org/10.1016/j.fuel.2018.08.062.

24. R. Haghniaz, A. Rabbani, F. Vajhadin, T. Khan, R. Kousar, A.R. Khan, H. Montazerian, J. Iqbal, A. Libanori, H.-J. Kim, Anti□bacterial and wound healing□promoting effects of zinc ferrite nanoparticles, Journal of nanobiotechnology. 19 (2021) 1-15, https://doi.org/10.1016/j.fuel.2018.08.062.

25. K.S. Park, Z. Ni, A.P. Côté, J.Y. Choi, R. Huang, F.J. Uribe-Romo, H.K. Chae, M. O'Keeffe, O.M. Yaghi, Exceptional chemical and thermal stability of zeolitic imidazolate frameworks, Proceedings of the National Academy of Sciences. 103 (2006) 10186-10191, https://doi.org/10.1073/pnas.0602439103.

26. S. Kanagesan, M. Hashim, S. AB Aziz, I. Ismail, S. Tamilselvan, N.B. Alitheen, M.K. Swamy, B. Purna Chandra Rao, Evaluation of antioxidant and cytotoxicity activities of copper ferrite (CuFe2O4) and zinc ferrite (ZnFe2O4) nanoparticles synthesized by sol-gel self-combustion method, Applied Sciences. 6 (2016) 184, https://doi.org/10.3390/app6090184.

27. X. Song, J. Mo, Y. Fang, S. Luo, J. Xu, X. Wang, Synthesis of magnetic nanocomposite Fe3O4@ ZIF-8@ ZIF-67 and removal of tetracycline in water, Environmental Science and Pollution Research. 29 (2022) 35204-35216, https://doi.org/10.1007/s11356-021-18042-9.

28. R. Geng, H. Tang, Q. Ma, L. Liu, W. Feng, Z. Zhang, Bimetallic Ag/Zn-ZIF-8: An efficient and sensitive probe for Fe3+ and Cu2+ detection, Colloids and Surfaces A: Physicochemical and Engineering Aspects. 632 (2022) 127755, https://doi.org/10.1016/j.colsurfa.2021.127755.

29. A.K. Yadav, P. Sirohi, S. Saraswat, M. Rani, M.P. Singh, S. Srivastava, N.K. Singh, Inhibitory mechanism on combination of phytic acid with methanolic seed extract of Syzygium cumini and sodium chloride over Bacillus subtilis, Current microbiology. 75 (2018) 849-856, https://doi.org/10.1039/c6en00136j.

30. G.V. Lowry, R.J. Hill, S. Harper, A.F. Rawle, C.O. Hendren, F. Klaessig, U. Nobbmann, P. Sayre, J. Rumble, Guidance to improve the scientific value of zeta-potential measurements in nanoEHS, Environmental Science: Nano. 3 (2016) 953-965, https://doi.org/10.1007/s00284-018-1457-5.

31. Haktanir I, Masoura M, Mantzouridou F T, et al. Mechanism of antimicrobial activity of honeybee (Apis mellifera) venom on Gram-negative bacteria: Escherichia coli and Pseudomonas spp[J]. AMB Express, 2021, 11(1): 1-11, https://doi.org/10.1186/s13568-021-01214-8.

32. C. Zhang, Z. Shu, H. Sun, L. Yan, C. Peng, Z. Dai, L. Yang, L. Fan, Y. Chu, Cu (II)@ ZIF-8 nanoparticles with dual enzyme-like activity bound to bacteria specifically for efficient and durable bacterial inhibition, Applied Surface Science. 611 (2023) 155599, https://doi.org/10.1016/j.apsusc.2022.155599.

33. S.J. Ko, M.K. Kim, J.K. Bang, C.H. Seo, T. Luchian, Y. Park, Macropis fulvipes venom component Macropin exerts its antibacterial and anti-biofilm properties by damaging the plasma membranes of drug resistant bacteria, Scientific Reports. 7 (2017) 16580, https://doi.org/10.1038/s41598-017-16784-6.

34. X. Ji, Y. Wu, Y. Han, B. Liang, Y. Cheng, J. Zheng, S. Guo, C. Li, H. Xu, Synergistic antibacterial study of nano-Cu2O/CuO@ Ag-tetracycline composites, Materials Chemistry and Physics. 306 (2023) 127904, https://doi.org/10.1016/j.matchemphys.2023.127904.

35. T.J. Silhavy, D. Kahne, S. Walker, The bacterial cell envelope, Cold Spring Harbor perspectives in biology. 2 (2010) a000414, https://doi.org/10.1101/cshperspect.a000414.

36. M. Godoy-Gallardo, U. Eckhard, L.M. Delgado, Y.J. de Roo Puente, M. Hoyos-Nogués, F.J. Gil, R.A. Perez, Antibacterial approaches in tissue engineering using metal ions and nanoparticles: From mechanisms to applications, Bioactive Materials. 6 (2021) 4470-4490, https://doi.org/10.1016/j.bioactmat.2021.04.033.

37. J.A. Lemire, J.J. Harrison, R.J. Turner, Antimicrobial activity of metals: mechanisms, molecular targets and applications, Nature Reviews Microbiology. 11 (2013) 371-384, https://doi.org/10.1038/nrmicro3028.

38. S. Soren, S. Kumar, S. Mishra, P.K. Jena, S.K. Verma, P. Parhi, Evaluation of antibacterial and antioxidant potential of the zinc oxide nanoparticles synthesized by aqueous and polyol method, Microbial pathogenesis. 119 (2018) 145-151, https://doi.org/10.1016/j.micpath.2018.03.048.

39. G. Applerot, N. Perkas, G. Amirian, O. Girshevitz, A. Gedanken, Coating of glass with ZnO via ultrasonic irradiation and a study of its antibacterial properties, Applied surface science. 256 (2009) S3-S8, https://doi.org/10.1016/j.apsusc.2009.04.198Get rights and content.

40. X. Wang, H. Wang, J. Cheng, H. Li, X. Wu, D. Zhang, X. Shi, J. Zhang, N. Han, Y. Chen, Initiative ROS generation of Cu-doped ZIF-8 for excellent antibacterial performance, Chemical Engineering Journal. 466 (2023) 143201, https://doi.org/10.1016/j.cej.2023.143201.

41. S.-C. Park, N.-H. Kim, W. Yang, J.-W. Nah, M.-K. Jang, D. Lee, Polymeric micellar nanoplatforms for Fenton reaction as a new class of antibacterial agents, Journal of Controlled Release. 221 (2016) 37-47, https://doi.org/10.1016/j.jconrel.2015.11.027.

42. J. Hu, H. Guo, J. Li, Q. Gan, Y. Wang, B. Xing, Comparative impacts of iron oxide nanoparticles and ferric ions on the growth of Citrus maxima, Environmental pollution. 221 (2017) 199-208, https://doi.org/10.1016/j.envpol.2016.11.064.

43. Wang J, Fang X, Chen H, et al. Antibacterial properties of the flower shaped nano-CuFe2O4@ MoS2 composites[J]. Colloids and Surfaces A: Physicochemical and Engineering Aspects. 683(2024) 133076, https://doi.org/10.1016/j.colsurfa.2023.133076.